Future variability of wave energy in the Gulf of Oman using a high resolution CMIP6 climate model

Mamoud Pourali [a,*], Mohamad Reza Kavianpour [a], Bahareh Kamranzad [b,c,d], Mohamad Javad Alizadeh[e]

[a] Faculty of Civil Engineering, K.N. Toosi University of Technology

[b] Hakubi Center for Advanced Research, Kyoto University, Yoshida Honmachi, Sakyo-ku, 606-8501, Kyoto, Japan

[c] Graduate School of Advanced Integrated Studies in Human Survivability (GSAIS), Kyoto University, Yoshida-Nakaadachi 1, Sakyo-ku, Kyoto 606-8306, Japan

[d] Department of Physics, Faculty of Natural Sciences, Imperial College London, London, SW7 2AZ, United Kingdom

[e] Caspian Sea National Research Center, Water Research Institute, Tehran, Iran

Corresponding author's email: m.pourali@email.kntu.ac.ir

Abstract

There is a worldwide compromise toward increasing the proportion of renewable energy in future electricity production to mitigate the impacts of greenhouse gases. This study explores the sustainability of wave energy resources in the northern part of the Gulf of Oman, considering the impact of climate change using a Shared Socio-economic Pathway (SSP5-8.5) representing a high increase in CO_2 concentration by 2100. Near-surface wind speed dataset from a high-resolution CNRM (CNRM-CM6-1-HR) global climate model was employed to force a third-generation wave model. A novel statistical bias-correction technique was developed based on Weibull distribution to generate high-resolution input wind for the wave model, and various criteria were employed to assess the sustainability of the wave energy in the study area. Comparing future projections of wave energy under SSP5-8.5 with those of historical simulations demonstrated the sustainability of the wave resources in the study area. The methodology of utilizing multiple criteria assessments, including accessibility, availability, and exploitable storage of wave energy predicts an increase ranging from 21 to 45% in the future wave power under a high emission scenario.

Keywords: Wave energy, Climate change, Weibull-based bias-correction, Gulf of Oman, Emission scenario

Nomenclature

General:

SSP	Shared Socio-economic Pathway
WEC	Wave Energy Converter
GCM	Global Circulation Model
IPCC	Intergovernmental Panel on Climate Change
CMIP6	Coupled Model Intercomparison Project Phase 6
SDGs	Sustainable Development Goals
ECMWF	the European Centre for Medium-Range Weather Forecasts
CNRM	Centre National de Recherches Meteorologiques
ERA	ECMWF Re-Analysis reanalysis
SW	Spectral Waves

Downscaling:

f(w)	Weibull probability distribution on wind components
We+	Existing bias-correction technique based on Weibull distribution
We*	Proposed bias-correction technique based on Weibull distribution
A	Scale parameters of the Weibull distribution
k	Shape parameters of the Weibull distribution
$A'(i)$	Modified scale parameters in the month i for the future period

$k'(i)$	Modified shape parameters in the month i for the future period

Hydrodynamic:

W	Speed of wind (m/s)
u	Eastward wind speed (m/s)
v	Northward wind speed (m/s)
H_s	Significant wave height (m)
T_p	Peak wave period (s)
C_d	White capping
k_n	Bed friction, Nikuradse roughness (m)
N	Action density
σ	Frequency (hz)
C	Propagation velocity (m/s)
θ	Wave direction (rad)
x	Spatial coordinate in eastward direction (m)
y	Spatial coordinate in northward direction (m)
t	Time (s)
S	Source term

Energy:

P	Wave power (kW/m)
H_s	Significant wave height (m)

T_e	Energy period (s)
P_{ave}	Mean power (kW/m)
E_t	Total storage of wave energy per area (kWh/m)
E_e	Exploitable storage of wave energy per area (kWh/m)
Exploitability %	E_t relative to E_e
SVI	Seasonal variability index
MVI	Monthly variability index
Statistic:	
Model Skill	Agreement index
SI	Scatter index
CC	Correlation coefficient
BIAS	Systematic differences between results and facts
RMSE	Root mean square error
X_m	Value of actual time series
X_p	Value of estimated time series
n	Number of data

1. Introduction

Wave energy as a clean and renewable energy resource is researched a lot because the majority of the human population lives in the vicinity of oceans and seas. However, it has not been commercialized yet and is still in progress. The selection of appropriate locations for energy extraction can play an important role in the efficiency of the Wave Energy Converters (WECs)

[1]. Formerly, it was deemed that locations with higher mean annual wave power are desirable, while less attention was paid to temporal variation of the power. Recently, it was found that locations with lower energy, but higher temporal stability are more favorable in terms of wave energy extraction compared to those with higher energy but less temporal stability [2]. [3] and [4] explored the performance of different wave energy converters at different installation depths and at different locations concluding that not only the suitable WEC type, but also the optimal design varies for different locations and depths. Along with intra-annual fluctuations, the future variation of wave energy resources due to changing climate may significantly affect the viability of the power extraction due to the increase in the greenhouse gas concentration. Therefore, many studies have been devoted to investigating the impacts of climate change on renewable energy resources [5–9].

Considering climate change impacts on renewable energy resources, it is important to take into account the trends in the current/past wave power and explore the possible future variations. Assessing the long-term behavior of wave conditions, [10] reported an increase in global wave power by 0.4% per year from 1984 to 2017. The results align with the other studies that demonstrated increasing wave energy trends for different regions [4] [11]. Global Circulation Models (GCMs) provide the future projections of various atmospheric and oceanic variables. These models are developed and run globally, considering several possible future scenarios. Following the latest updates of the Intergovernmental Panel on Climate Change (IPCC) released as Coupled Model Intercomparison Project phase 6 (CMIP6), the model projecting climatic variables is developed according to Shared Socio-economic Pathways (SSPs). Wind resource evolution under different CMIP6 climate change scenarios in Europe and North America has been investigated by [12] and [13]. However, wave characteristics are not projected in GCMs, directly. Thus, the wind field obtained from GCMs is utilized as a driving force to wave models to generate the wave characteristics and subsequently, investigate the wave resources. Since GCMs commonly run at a coarse spatial resolution which may not cover the local fluctuations, bias-correction or downscaling processes may be required for regional studies. Regionalization of GCM simulations is a common practice to achieve more reliable results consistent with the conditions governing the area.

Regression models, artificial intelligence models, quantile mapping models and Weibull distribution models are all already used for wind field modifications [14], [15]. Based on a comparison of the performance of different statistical downscaling techniques, including multiplicative shifting, quantile mapping, support vector regression, and Weibull-based techniques, the Weibull-based technique outperformed them all [15]. This method is based on the probability distribution of the wind components and simultaneously modifies wind speed and direction. Moreover, the method does not disturb the sequential order of time series, which are important in wave power projections. However, there is still a need for improvement and progress to enhance the efficiency and accuracy of the method. In fact, since the Weibull equation is inherently in a multiplicative form because of a coefficient called the shape factor, using the multiplicative relation will improve the estimates compared to the additive method. Because of their strong dependence and sensitivity on the wind field, choosing and applying a suitable bias-correction technique is crucial to the accuracy and viability of wave projections. [16].

In order to select the appropriate locations and WECs for wave energy extraction, it is vital to consider various criteria in line with the sustainability of the resources. The suitability of less powerful but more consistent wave resources has been addressed by [17] and [18]. In addition, the authors discussed different factors influencing the optimal site selection for wave energy farms. Assessment of renewable energy resources in Iran with a focus on marine resources has revealed many energy hotspots with a high potential for marine energy development [19]. The Gulf of Oman, with its vicinity to the Indian Ocean and the swells traveling from the Southern Ocean, has the potential to supply part of the energy demands for the population living in the coastal areas. More importantly, there are several coastal villages far from the cities where access to electricity is limited. In addition, with its proximity to the Indian Ocean and access to open waters, the Gulf of Oman is an attractive location for various industrial projects and developments, whereas the complex sea state is highly affected by both Shamal and monsoon winds from the west and south, respectively [16] and makes the spatio-temporal analysis required. Considering the local energy resources such as wave energy, it can be considered a cost-effective and sustainable choice for the electricity supply. There have been previous studies on the investigation of wave energy resources in the Gulf of Oman, such as [20,21], in which the analysis has been done based only on the mean wave energy values and their variability on a monthly scale. In addition, [22] proposed a multi-criteria approach to select the most appropriate combination of wave energy convertor and location in several stations in the Caspian Sea, the Persian Gulf, and the Gulf of Oman. They used different factors, including exploitable storage of energy, accessibility, availability, energy production, design wave height, and intra-annual variation of the resources. However, their analysis has been done only based on the historical simulation of wave characteristics and lacks long-term changes due to climate change.

The main objective of this study is to develop an accurately modeled wave field to estimate the future wave power conditions in the northern part of the Gulf of Oman. For this purpose, the wind dataset of SSP5-8.5 derived from a CMIP6 model is modified by developing a Weibull distribution based. Afterward, the modified wind field is used to run the third-generation model MIKE 21 Spectral Waves (SW) [23] to obtain wave characteristics. Following the proposed approach based on different criteria, the sustainability of wave energy resources under the impact of climate change is investigated in four locations. In section 2, the methodology includes study area, calibration, climate data, numerical wave model characteristics, the proposed downscaling technique, modeling procedures, and wave power computations. Results are presented in section 3, while a discussion is given in section 4. The main findings and conclusions are summarized in section 5.

2. Materials and methods

The methodology of this study is described as: selection of specific locations in the study area, collecting the dataset, modification of wind field derived from the climate model, performance evaluation of the numerical wave model, calculation of wave power, and assessing the climate change impact on wave energy and temporal stability analysis. In climate change impact studies, it is common to investigate future projections in either the near or far future (e.g. [24]). Considering the goal of this study to focus on the sustainability of resources in the long-term and in order to further compare the results with additional relevant studies, a period of 100-year has been selected. Four points in the northern Gulf of Oman have been chosen for site selection. Two datasets, including the near-surface wind speed of ERA5 reanalysis dataset [25] from 1981 to 2000, and also historical wind speed (1981-2000) and future (2081-2100) scenario of SSP5-8.5 from CMIP6 CNRM climate model [26], were used. The dataset was selected since it has the highest spatial resolution among the available GCMs. The area is affected by various climates, such as monsoons from the Indian Ocean and shamal wind from the northwest to some extent. Hence, high-resolution wind data plays an important role in not only generating higher accuracy wave height and period but also a correct propagation direction. The CNRM data are bias-corrected (considering ERA5 as the reference dataset for the historical period) by developing an improved statistical technique based on Weibull distribution. The modified data of wind components are used to run the numerical wave model for both historical and future periods. To estimate the wave energy, the numerical wave model (MIKE21 SW) results are used. Finally, different analyses are carried out to explore climate change impacts and wave energy variability in the long term at the selected locations.

2.1. Study area and data

The selected locations in this study include four spots in the northern Gulf of Oman in the nearshore areas of Iranian waters. The Chabahar free trade-industrial zone is located there where it is experiencing fast growth and subsequently increasing demand for energy production. Moreover, there are rural and urban regions nearby the Gulf, where the development of local energy sources can be economically viable and reduce the cost of long-distance energy transfer from a power plant to the consumption units. Regarding the population and the importance of these regions, four points (P1 to P4) as candidate locations are selected for wave energy analyses, as illustrated in Fig. 1 and Table 1. Moreover, distance from the residential areas to the energy sources was also considered in selecting the locations. It should be noted that the computational domain in both wind calibrating and wave simulation includes a rectangular area covering the longitudes 47.5°E-74.0°E and latitudes 15.0°N-30.5°N. It covers the Gulf of Oman above 15° latitude to the Persian Gulf. The target area of the modeling is shown in Fig. 1.

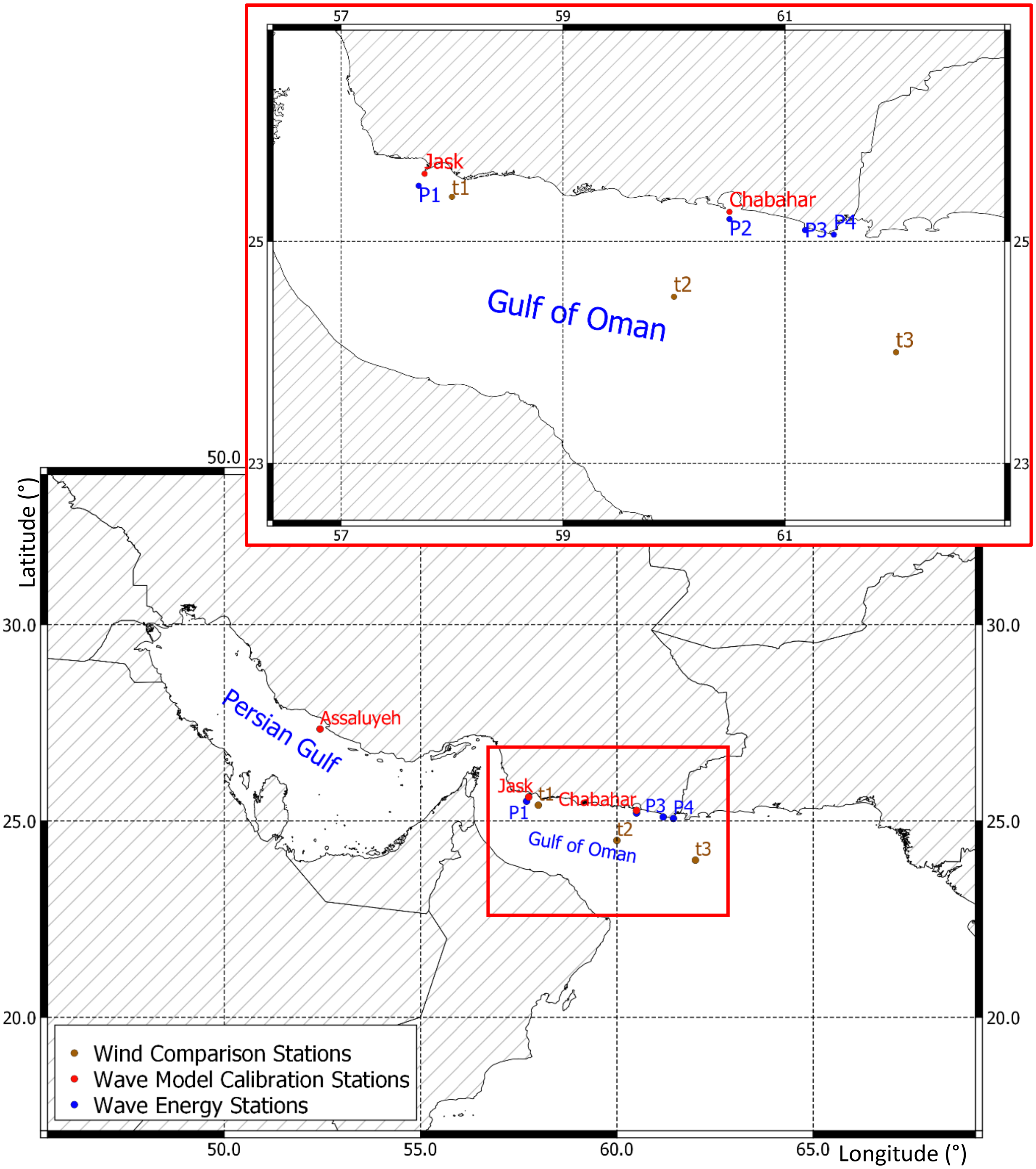

Fig. 1. Study area, wind comparison spots, and selected wave energy locations

Table 1. Locations of the selected spots for wave analysis

Point	Location	Long. (°)	Lat. (°)	Depth [m]
P1	Jask	57.7	25.5	100
P2	Chabahar	60.5	25.2	55
P3	Beris	61.18	25.1	14
P4	Pasabandar	61.44	25.06	30

2.2. Reanalysis and climate model datasets

Two sets of data have been used for the wave climate investigation in the study area. Eastward and northward wind components of ERA5 reanalysis with a spatial resolution of 0.25°×0.25° and temporal resolution of 1 hour have been downloaded from https://cds.climate.copernicus.eu/ and were used as the reference data for bias-correction of the wind field obtained from the CMIP6 GCM. The data was obtained for the whole computational domain for 20 years, from 1981 to 2000. Skill assessment and validation of ERA5 reanalysis dataset against measurements and altimeter observations indicated its efficiency for wind field simulation over the study area [27][28]. Moreover, several studies in different areas applied ERA5 and its previous versions developed by ECMWF, as reference data for downscaling/bias-correction of GCMs on a local scale [21,29–31].

Wind speed characteristics as an input to the wave model are necessary to evaluate future variability in wave power. In CMIP6 models, the climate variables for the future period are available for different SSPs. In this regard, four SSPs; SSP1-2.6, SSP2-4.5, SSP3-7.0, and SSP5-8.5 are used for climate change studies [32]. According to the purpose of this study which is to explore the future variability of the wave power under climate change impacts, the wind speed simulation of the scenario SSP5-8.5 is considered for future wave power projection. SSP5-8.5 is a high emission scenario which is an updated version to CMIP5 RCP8.5, indicating radiative forcing of 8.5 W/m^2 by 2100, and it assumes a fossil-based economy in the future. SSP5-8.5 is a pessimistic socio-economic pathway scenario exacerbating future changes due to a rapid increase in CO_2 concentration. Finally, the worst-case scenario (SSP5-8.5) is expected to result in the highest variability in the future atmospheric conditions than the other scenarios. Thus, it is important to consider such variations for future planning and management. In addition, many studies on climate change impacts on wave climate have used RCP8.5 (the equivalent of SSP8.5 in CMIP5 models) [33], [24], and [8]. Hence, this study focuses on using this scenario for future projections.

The next step is to select an appropriate GCM with reliable performance in the study area, considering its spatio-temporal resolution and coverage. To that end, GCM evaluation is a common task to find the climate model with the best performance for a particular area [34]. Following the previous studies and also due to the high spatial resolution, the CNRM-CM6-1-HR outputs have been selected in this study [35]. Thus, near-surface wind speed of the historical (1981-2000) and future period (2081-2100) from the CNRM model have been obtained and assessed. The data has a temporal resolution of 3 hours and spatial resolution of 0.5°×0.4993° for both historical and future periods. Fig. 2 illustrates the mean annual wind speed for ERA5 and CNRM-CM6-1-HR model over the computational domain from 1981 to 2000. This figure shows a bias in the wind speed simulations obtained from the GCM compared with ERA5, especially in the southern parts of the Gulf of Oman when it is connected to the Indian Ocean.

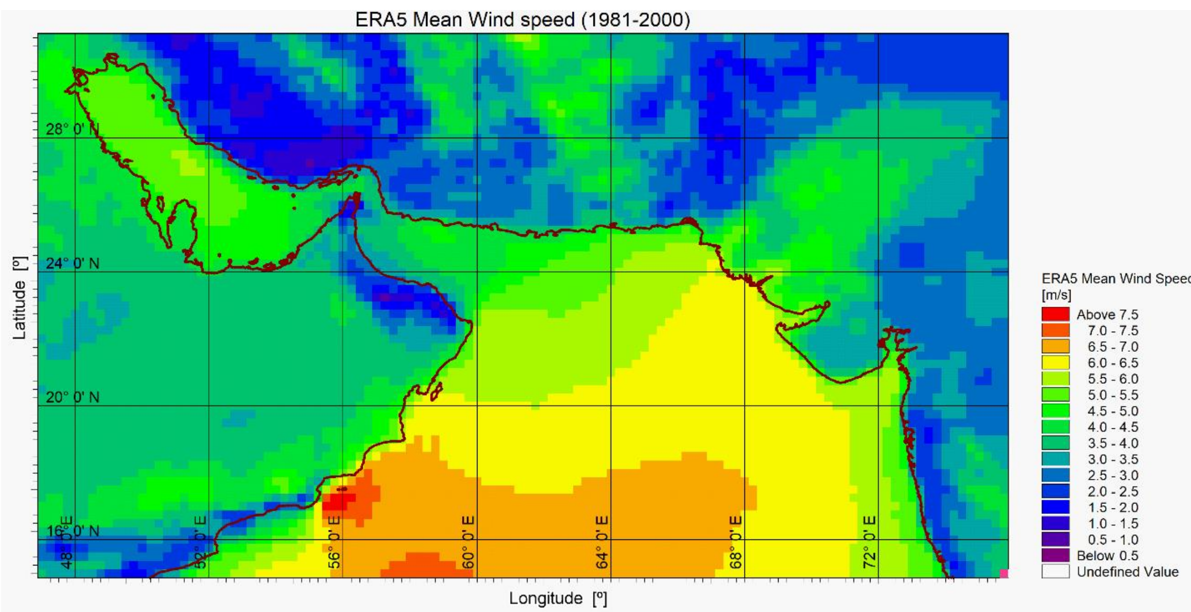

a)

b) 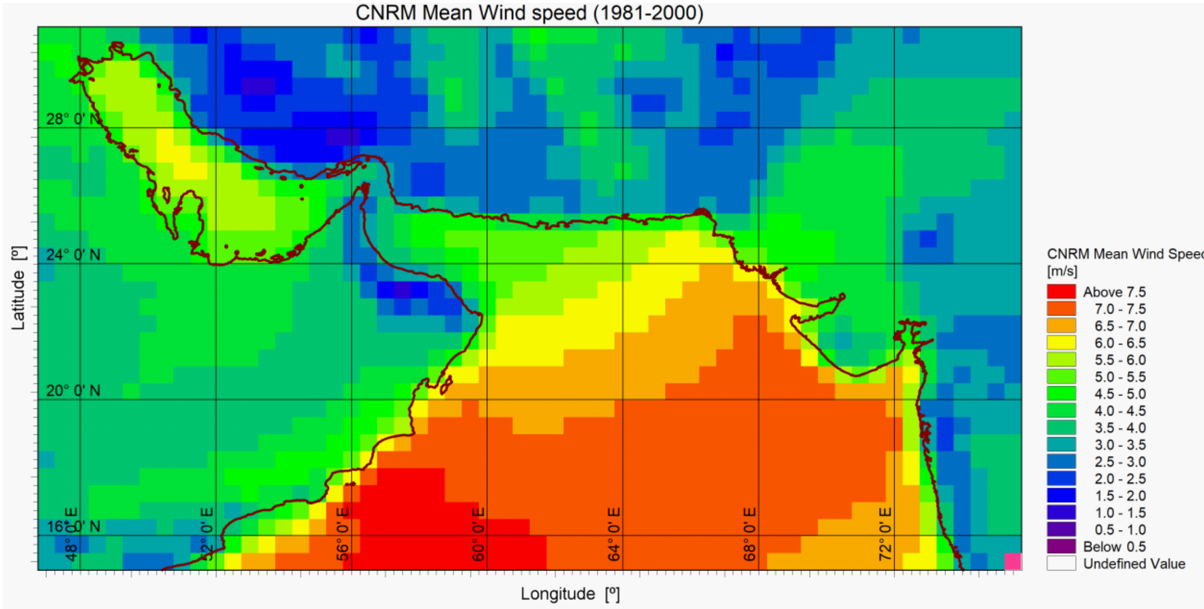

Fig. 2. Mean annual wind speed for historical period (1981-2000) a) ERA5, b) CNRM

As shown in Fig. 2, the GCM used in this study (CNRM) needs to be modified to resemble the wind field on the regional scale properly, and modifications are required in order to increase the accuracy of the wind data. Table 1 presents the statistical characteristics of the ERA5 and CNRM wind speed simulations in the selected locations (P1 to P4) for the historical period. The statistics in Table 2 show that the CNRM model overestimates the wind speed for the selected locations in terms of minimum, maximum, average, and standard deviation calculated for 20 years. The standard deviation is also higher for the wind speed derived from CNRM. Hence, bias correction is required before applying the CNRM outputs for wave climate projection, assuming that the same correction method is applied to the future dataset.

Table 2. Statistics of the wind speed data from ERA5 and CNRM (1981 to 2000)

Station	ERA5				CNRM			
	Min.	Max.	Avg.	Std.	Min.	Max.	Avg.	Std.
Jask	0.06	14.852	4.645	2.236	0.139	18.169	4.946	2.634
Chabahar	0.068	15.618	4.144	1.904	0.087	24.059	4.471	2.302
Beris	0.146	15.087	4.053	1.855	0.149	23.824	4.314	2.221

Pasabandar	0.117	14.515	4.070	1.881	0.183	24.070	4.405	2.267

2.3. The proposed bias-correction technique

In this study, an improved version of the Weibull-based technique as a statistical bias-correction approach is employed to modify the wind field. The initial version of this technique was proposed by [15] to fit Weibull probability distribution on wind components through a data-transformation process. Generally, Weibull distribution can be defined as:

$$f(W) = \frac{k}{A}(\frac{W}{A})^{k-1}\exp\,[-(\frac{W}{A})^{k}] \quad (1)$$

Where W is the speed of wind and A and k are called scale and shape parameters of the distribution. Following Eq. (1), it can be found that the distribution is dependent on these two parameters and having the time series of wind speed, the main practice is to find them through the standard deviation method or alternatively by means of the maximum likelihood method [36]. Weibull (shape and scale) parameters of the historical datasets of ERA5 and CNRM model for each gridpoint are compared, and their ratio is used as a correction factor to modify the wind field in the future period for SSP5-8.5. These coefficients can be obtained as Eqs. (2-3) and employed for future wind field modifications as Eqs. (4-5).

$$D_{A(i)} = A^{His}_{ERA5(i)} / A^{His}_{CNRM(i)} \quad (2)$$

$$D_{k(i)} = k^{His}_{ERA5(i)} / k^{His}_{CNRM(i)} \quad (3)$$

$$A'^{Future}_{CNRM(i)} = A^{Future}_{CNRM(i)} * D_{A(i)} \quad (4)$$

$$k'^{Future}_{CNRM(i)} = k^{Future}_{CNRM(i)} * D_{k(i)} \quad (5)$$

Where $A(i)$ and $k(i)$ are the modified scale and shape parameters in the month i for the future period. In comparison with the previously proposed method [15], in which the difference was used as the correction coefficient, this study uses the proportion of the Weibull parameters in the historical period for the two datasets. An attempt is made to examine and compare the multiplicative form against the difference form as an alternative.

The efficiency of the proposed bias-correction technique depends on the assumption that the wind field in the region follows a Weibull distribution. As previous studies showed, in the study area, Weibull distribution fits suitably with the wind data. Therefore, a distribution-based model can be beneficial to both modifying the data statistics and the probability distribution of the data. Moreover, the application of the Weibull distribution is limited to positive values of $W \geq 0$ where wind components (u and v representing eastward and northward wind speeds) can be either positive or negative depending on the direction they show. Therefore, the data transformation process should be implemented on the wind components before fitting the distribution. The scheme for data transformation is adding the absolute of the strongest wind components (u, v) with a negative sign to the time series of the same point and the same component. Although the transformation may introduce an irreversible error, the efficiency of this method is still advantageous to the traditional approach of applying the Weibull distribution on the wind speed (W) directly. This is mainly due to wind speed and direction modification when wind components are improved. It is noted that the suitability of the Weibull distribution on the transformed wind components is checked throughout the bias-correction process. More information concerning the validity of the Weibull-based model can be found in [15].

The Weibull distribution is fitted on wind components (u, v) individually. The shape and scale parameters are computed for the historical period of the reference and GCM wind components. Afterward, the correction factor is obtained from the historical datasets (Eqs. 2 and 3) and multiplied by the corresponding shape and scale factors values in the future periods (Eqs. 4 and 5). Finally, wind components are modified and subsequently de-transformed to their original ranges utilizing the modified parameters and inverse Weibull distribution. This procedure is repeated for all the gridpoints, one by one, using a distributed scheme to modify the wind field over the whole computational domain. The modified wind field can be used as input for the numerical wave model to generate the wave characteristics and, consequently, the wave power.

2.4. Numerical wave model

In this study, MIKE 21 SW, a third-generation spectral numerical model based on unstructured meshes, is employed to simulate wave characteristics in historical and future periods. The model has been successfully applied for nearshore and offshore wave modeling [37–40]. It uses a spectral action balance equation considering the growth, decay, and transformation of wind-generated waves and swells in offshore and coastal areas to simulate wave evolution [23]. The basic equation can be formulated either in the Cartesian coordinates for small-scale applications and polar spherical coordinates for large-scale applications. Thus, for this study, the wave action balance equation is written in spherical coordinates as:

$$\frac{\partial N}{\partial t} + \frac{\partial}{\partial \phi} C_{\phi} N + \frac{\partial}{\partial \lambda} C_{\lambda} N + \frac{\partial}{\partial \sigma} C_{\sigma} N + \frac{\partial}{\partial \theta} C_{\theta} N = \frac{S}{\sigma} \quad (6)$$

Where N is the action density, t is time, ϕ is the latitude, λ is the longitude, σ is frequency, C is the propagation velocity, and θ is wave direction in a nautical convention. The first three terms on the left side of Eq. (6) show temporal and spatial variation of N. The fourth term represents how the relative frequency changes as depth changes, while the fifth term represents refraction caused by depth and currents. The total source and sink function is represented by S reflecting the effects of the generation by wind, dissipation (by white-capping, depth-induced wave breaking, and bottom friction) and nonlinear wave-wave interactions [41]. Since MIKE 21 SW is embedded in two different formulations, including fully spectral and directional decoupled parametric formations, in this study, the fully spectral formulation is used based on the wave action conservation equation [23,42]. Figure 3 shows the computational wave domain, the size of the elements, and the bathymetry of the prepared wave model.

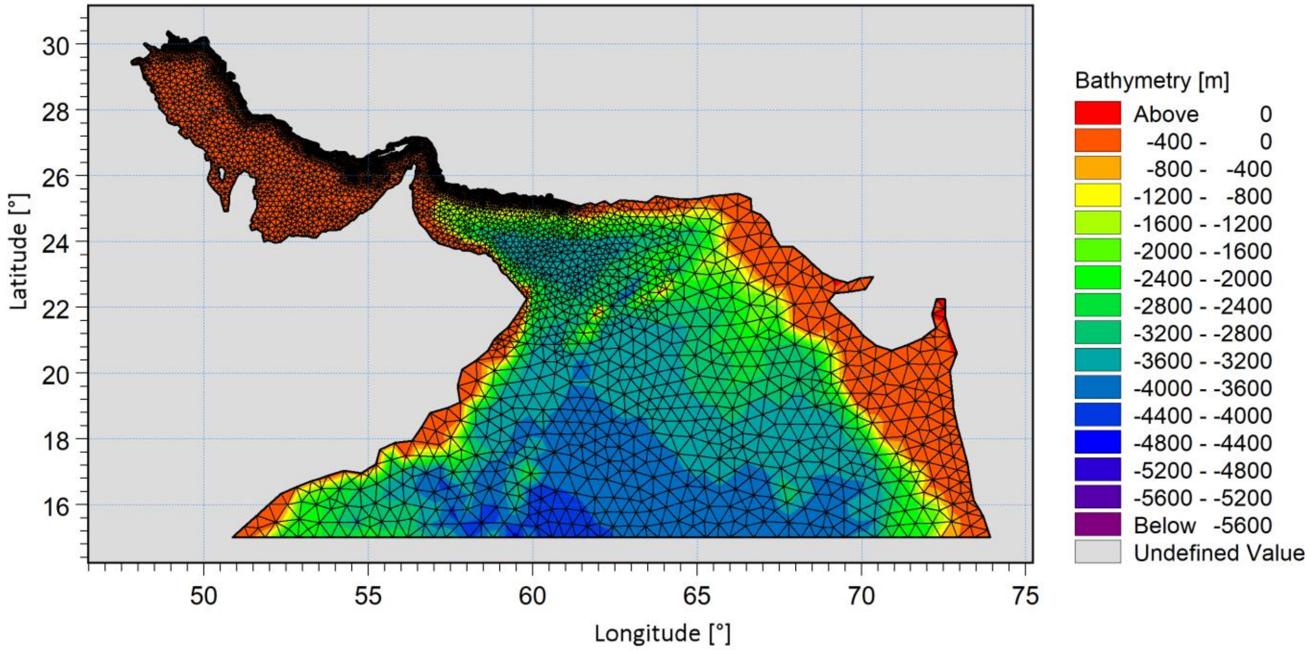

Fig. 3. Wave modeling domain, element size, and bathymetry of the wave model

The following statistical relationships were used to evaluate the wave model. They are among the standard statistical metrics to evaluate the accuracy of the model simulations. Generally, models with relatively higher $Model\ Skill$ and CC (closer to 1), but with lower $SI, RMSE$, and $BIAS$ are desirable. Table 3 shows the results of the wave model evaluation based on these formulas in Assaluyeh, Jask, and Chabahar stations.

$$Model\ Skill = 1 - \frac{\sum(X_p - X_m)^2}{\sum(|X_p - \overline{X_m}| + |X_m - \overline{X_m}|)^2} \quad (7)$$

$$SI = \frac{\sqrt{\frac{1}{n}\sum(X_p - X_m)^2}}{\overline{X_m}} \quad (8)$$

$$CC = \frac{\sum(X_p - \overline{X_p})(X_m - \overline{X_m})}{\sqrt{\sum(X_p - \overline{X_p})^2 \sum((X_m - \overline{X_m})^2}} \quad (9)$$

$$BIAS = \sum \frac{1}{n}(X_p - X_m) \quad (10)$$

$$RMSE = \sqrt{\frac{1}{n}\sum(X_p - X_m)^2} \quad (11)$$

where X_m and X_p are the actual and the estimated time series, respectively. $\overline{X_m}$ and $\overline{X_p}$ are the average of the real and simulated values. Moreover, n denotes the number of the data, and the overbar indicates the sample mean.

2.5. Factor to assess the stability and suitability of resources

The outputs of the numerical wave models are available as significant wave height and wave period. Hence, to calculate the wave power (kW/m), deep water approximation was utilized [43,44]:

$$P \approx 0.49 H_s^2\, T_e \quad (12)$$

where H_s is the significant wave height and T_e is the energy period, which is a function of spectral moments of order *0* (m_0) and *-1* (m_{-1}) as follow:

$$T_e = \frac{m_{-1}}{m_0} \quad (13)$$

Using the wave power value for each time step, the mean power (P_{ave}) is calculated. Also, having the total hours per year (t), the total and exploitable storages of wave energy per unit area (E_t and E_e, respectively) can be obtained as:

$$E_t = P_{ave} \times t \quad (14)$$

$$E_e = P_{ave} \times t_e \quad (15)$$

Where t and t_e represent the total hours all year round and the total hours when the energy is greater than a threshold, respectively. The annual electric power production of a WEC device is calculated via a coupling of the device's power matrix and the wave resource matrix [45][46]. In this study, the threshold is considered 2 kW/m as suggested and applied by [45,47,48]. Moreover, extreme events are excluded in the calculations considering an upper limit for significant wave height as $H_s \geq 4m$ [49]. Ratio of E_e to E_t is used as *exploitability*:

$$Exploitability\ (\%) = \frac{E_e}{E_t} \tag{16}$$

Since this study aims to evaluate the viability and sustainability of wave power under a high emission scenario (SSP5-8.5), intra-annual variability (monthly and seasonal variability) and availability must be considered. These factors depend on wave conditions that may change under the climate change impacts. It is worth mentioning that accessibility is another sea state-dependent factor that has been missed in this study since it was shown by [22] that accessibility reaches about 100% for Govatr located in the study area. Availability represents the percentage of time in which the wave characteristics lie in the desirable range of wave energy devices to operate efficiently. The range is restricted by cut-in and cut-off values of significant wave height, which are considered 0.5 *m* and 4 *m*, respectively, according to [50].

Seasonal and Monthly Variability Indices (*SVI* and *MVI*, respectively) are used to assess the temporal stability of both historical and future periods.

$$SVI = \frac{P_{S1} - P_{S4}}{P_{ave}} \tag{17}$$

$$MVI = \frac{P_{M1} - P_{M12}}{P_{ave}} \tag{18}$$

where P_{S1} and P_{M1} represent the mean wave power for the highest energy season and month, respectively, while P_{S4} and P_{M12} represent the mean wave power for the least energetic season and month, respectively. The annual mean wave power is denoted by P_{ave}. Generally, higher values of mean wave power and also lower values of *MVI* and *SVI* demonstrate more temporally stable conditions. Comparing the mentioned variables in the historical simulations with those of the future projection can provide the required information for decision-makers and authorities to have a suitable development plan considering the Sustainable Development Goals (SDGs).

3. Results

3.1. Wave model calibration and validation

To calibrate the numerical wave model, firstly, sensitivity analyses were conducted to find the most effective parameters on the model outputs. Subsequent to the mesh size optimization through the sensitivity analysis, white capping and bed friction were considered as the calibration factors. In case of white capping, the two parameters of C_d and $delta$ should be tuned accordingly. The bed friction can be specified with Nikuradse roughness parameter (k_n). After trial and error, the values of 2, 0.5, and 0.001 were selected for C_d, $delta$ and Nikuradse roughness, respectively. In terms of directional discretization and time formulation, 16 directions (22.5° resolution) and an instationary formulation were used. The evaluation was based on the model's capability to simulate the significant wave height (H_s) and peak wave period (T_p) in Assaluyeh, Jask and Chabahar where the observational records are available, while the wind field of ERA5 as the input to force MIKE 21 SW. Fig. 4 illustrates the time series of the numerical wave model versus the observational data for the three stations.

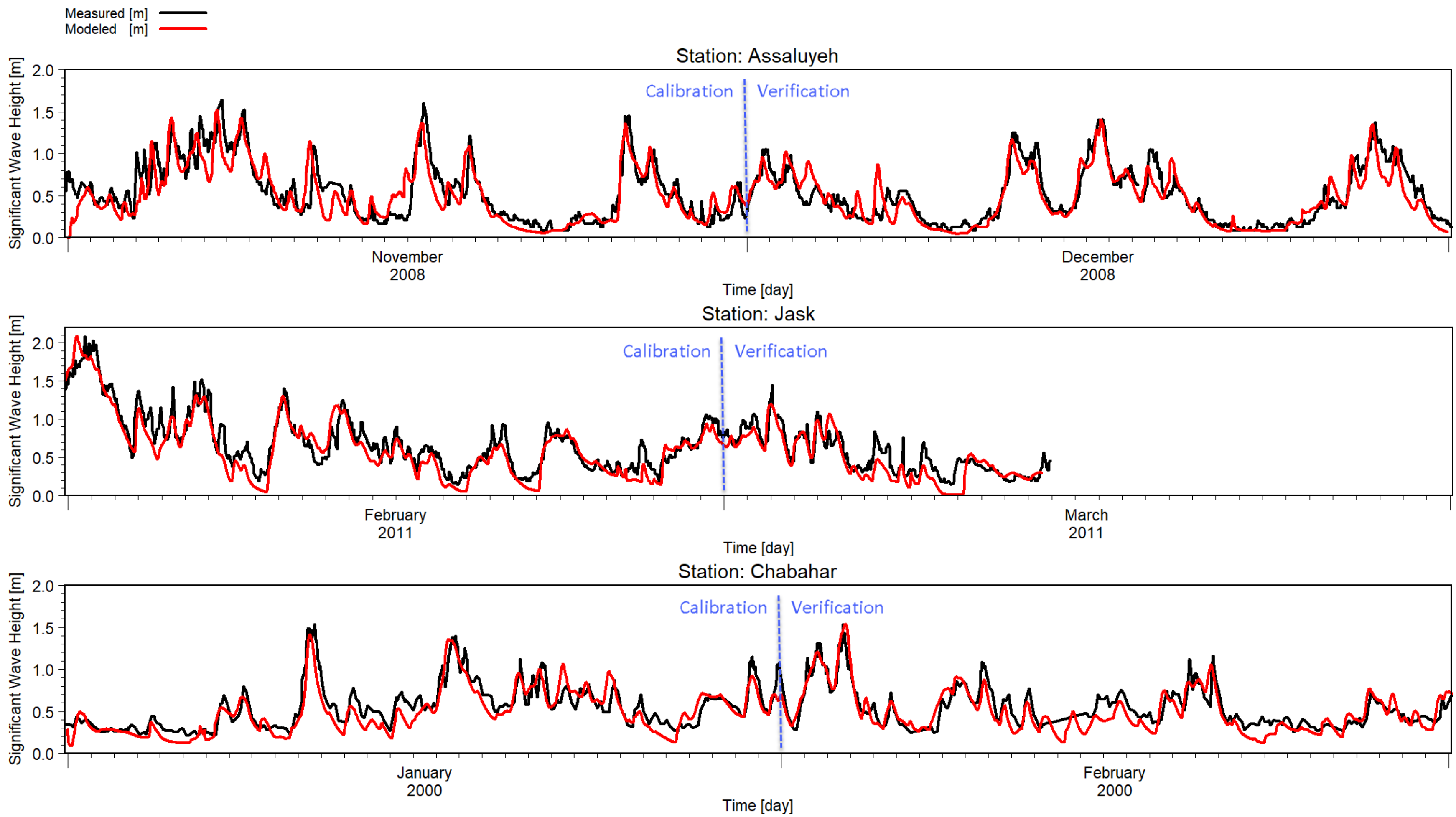

Fig. 4. Time series of the significant wave height (H_s) for the numerical model and observations in Assaluyeh, Jask, and Chabahar stations

Table 3. Simulation statistics of the significant wave height (H_s) in meters and peak wave period (T_p) in seconds

Buoy	Assaluyeh		Jask		Chabahar	
Data Period	Nov & Dec-2008		Feb & Mar-2011		Jan & Feb-2000	
Parameter	T_p	H_s	T_p	H_s	T_p	H_s
Model Skill	0.96	0.93	0.86	0.90	0.94	0.95
SI	0.19	0.35	0.17	0.34	0.11	0.22
CC	0.92	0.86	0.75	0.84	0.90	0.91
BIAS	-0.14	-0.03	-0.03	-0.08	0.02	-0.05
RMSE	0.76	0.18	0.76	0.21	0.13	0.15

According to Fig. 4 and Table 3, the observed and simulated wave heights coincide at all three stations. Values of error indices confirm the efficiency of the model. Therefore, the calibrated model can be employed to simulate the significant wave height in the area for a longer term.

3.2. Bias-correction of the wind field

The performance of the numerical wave models strongly depends on the accuracy of the wind field and its consistency with the local conditions. As mentioned earlier, bias correction is required for modifying the wind field obtained from the climate model. In this section, the performance of the proposed bias-correction technique has been provided in Table 4. Moreover, the results are compared with the recently developed bias-correction technique but with newly proposed modification criteria, as explained in section 2.3. It is pointed out that $We+$ stands for the existing bias-correction technique based on Weibull distribution, and $We*$ is the proposed method in this study which is a modified version of the $We+$ technique. In this comparison, sample points of t1, t2, and t3 belong to the area close to the Strait of Hormuz in the Gulf of Oman (Fig. 1).

Table 4. Performance of the developed bias-correction technique for the wind speed (compared with ERA5)

Location	t1			t2			t3		
	Long.(°) 58		Lat. (°) 25.4	Long. (°) 60		Lat. (°) 24.5	Long. (°) 62		Lat. (°) 24
Technique	Raw	*We+*	*We**	Raw	*We+*	*We**	Raw	*We+*	*We**
SI	0.80	0.667	0.666	0.78	0.629	0.629	1.24	0.589	0.589
CC	0.06	0.195	0.196	0.03	0.155	0.156	0.016	0.463	0.467
BIAS (m/s)	0.58	-0.169	-0.169	0.66	0.043	0.040	2.22	-0.108	-0.113
RMSE (m/s)	2.79	2.313	2.311	3.39	2.716	2.714	3.96	1.881	1.872

Along with the metrics presented in Table 4, the capability of the bias-correction technique to suitably resemble extreme events is of great importance and useful for many practical applications. In this regard, 95th and 99th percentile as indicators for extreme values of the wind speed for a 20-year period were calculated for the reference data and modified wind field obtained by implementing the bias-correction technique on the data from the climate model. Table 5 compares the efficiency of the proposed bias-correction technique with the existing technique in terms of 95th and 99th percentiles. It is pointed out that ERA5 is considered as the reference dataset to evaluate the performance of the bias-correction techniques.

Table 5. Performance of the bias-correction techniques to estimate extreme wind speeds

95th and 99th percentile of wind speed								**Absolute difference with ERA5**			
t1								**t1**			
95th percentile				**99th percentile**				**95th percentile**		**99th percentile**	
ERA5	Raw	We+	We*	ERA5	Raw	We+	We*	We+	We*	We+	We*
6.699	8.2	6.771	6.751	8.025	10.67	8.584	8.566	0.0725	0.0524	0.5589	0.5411
t2								**t2**			
95th percentile				**99th percentile**				**95th percentile**		**99th percentile**	
ERA5	Raw	We+	We*	ERA5	Raw	We+	We*	We+	We*	We+	We*

7.838	9.90	8.319	8.307	9.956	12.8	10.538	10.555
t3							
95th percentile				**99th percentile**			
ERA5	Raw	We+	We*	ERA5	Raw	We+	We*
6.381	10.4	6.552	6.533	8.016	12.9	8.584	8.513

0.4819	0.4697	0.5814	0.5990
t3			
95th percentile		**99th percentile**	
We+	We*	We+	We*
0.1711	0.1523	0.5674	0.4967

As observed from Table 5, the GCM simulations (here indicated as Raw) overestimate wind speed in terms of 95th and 99th percentiles for all the selected locations. Comparing the extreme values calculated from the modified wind field by the two bias-correction techniques indicates that the proposed method slightly outperforms its former counterpart. Moreover, there is consistency between the extreme values obtained from the reference data with those of the corresponding values calculated from the modified wind field of the climate model. Considering the absolute difference between the extreme values of ERA5 and the modified wind fields using the bias-correction technique, slightly lower errors (improved accuracy) are represented by the proposed bias-correction technique than the previous method. The proposed bias-correction technique remarkably improves climate models' wind speed in which the modified wind field is compatible with the reference data. As stated by [29], the additive correction of the Weibull parameters leads to significant improvement of the wind direction. To assure suitability of the developed method in this study, which is the multiplicative correction of the parameters, wind roses for the three locations are depicted for reference data and modified wind field from the climate model by additive and multiplicative correction factor (Fig. 5).

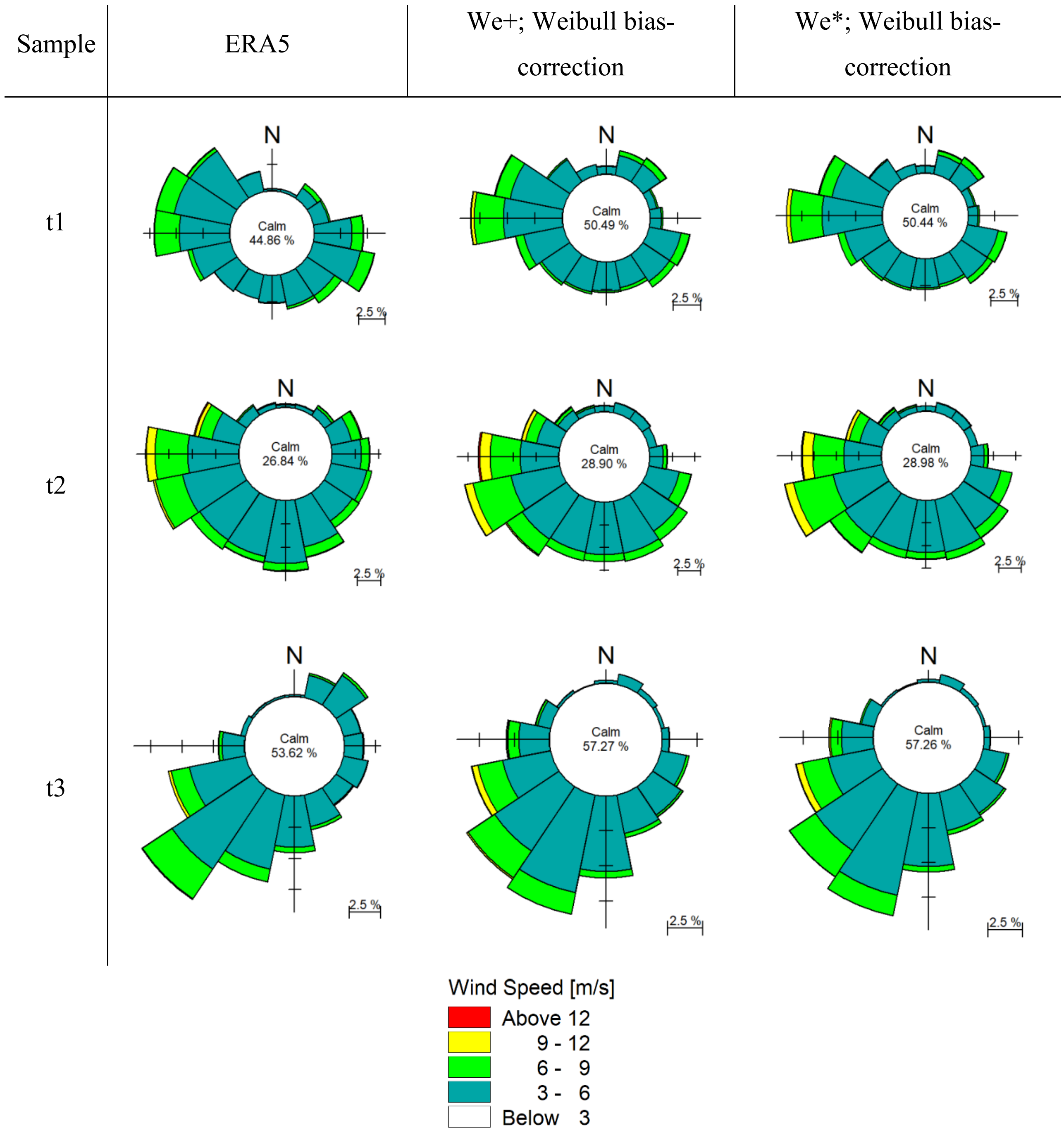

Fig. 5. Wind roses for different locations

Following Fig. 5, it is inferred that the directional distribution of the wind speed obtained from the two bias-correction techniques is nearly similar. Furthermore, similarity in magnitude and directions of wind speed for the reference data and modified data reveal the efficiency of the bias-correction technique. Considering the capability of the bias-correction technique to modify directional and magnitude distributions of the wind for the historical period as a validation stage, it can also be applied to the future wind field. Afterward, they can be employed for wave power projection to assess climate change impacts.

3.3. Historical and future exploitable wave energy

The calibrated wave model is employed for the future wave power projection. In this regard, the correction coefficient obtained for the historical wind field is applied to modify the future wind field representing the high emission SSP5-8.5 of the CNRM model. Climate change impacts can be investigated by comparing the historical and future wave power in the selected locations. Fig. 6 illustrates the spatial distribution of mean wave energy over the study area.

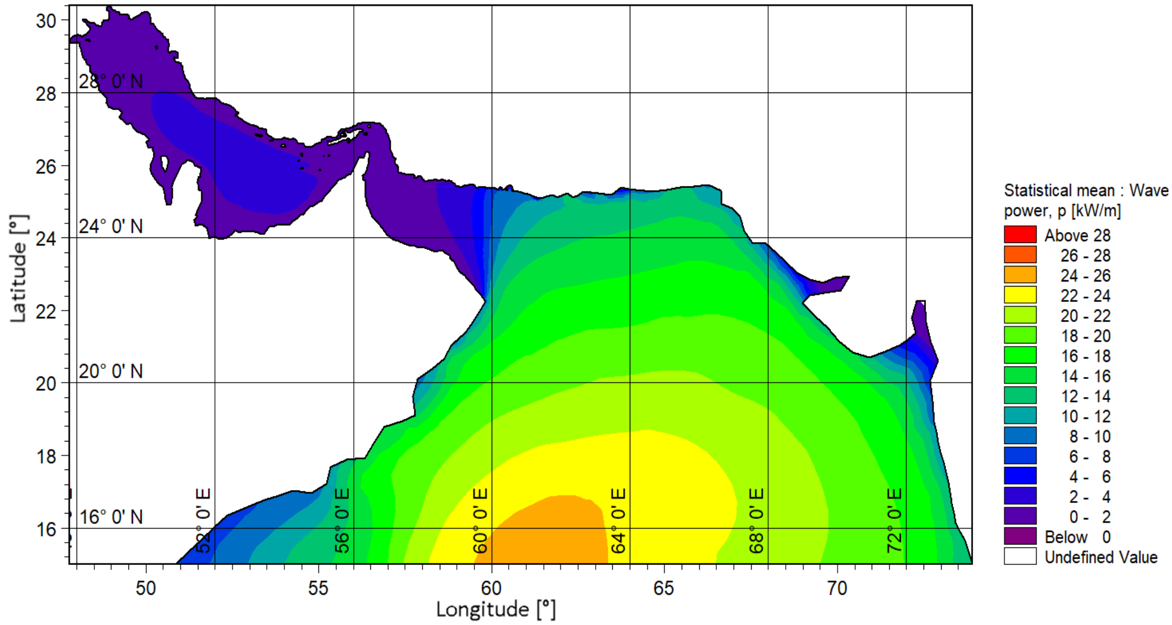

a)

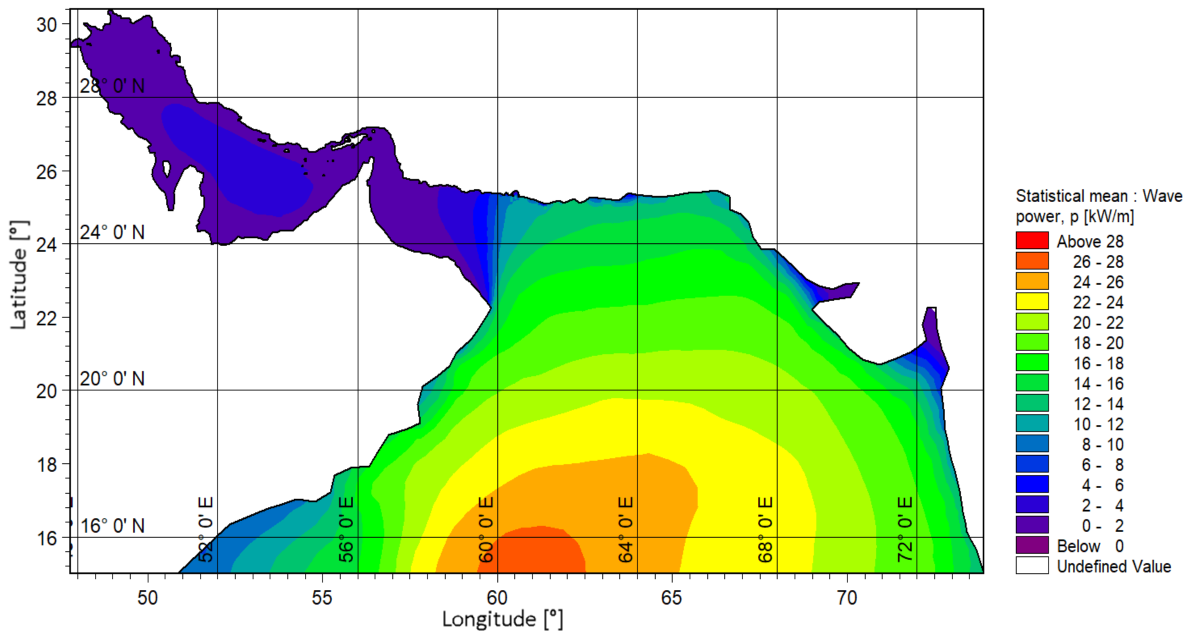

b)

Fig. 6. Spatial distribution of mean wave energy for the a) historical (1981 to 2000) and, b) future periods (2081-2100)

As observed from Fig. 6, the wave energy over the study area shows a great degree of variability where the offshore and eastern parts of the gulf are prone to more energetic waves. Regarding the future scenario, an increasing trend in wave energy can be observed over the study area. Four locations along the northern part of the gulf have been selected to provide more in-depth analysis of energy variability. They were considered according to the spatial distribution of wave energy, distance from the coasts, vicinity to the industrial or residential regions, etc. Hence, the computations were carried out for the total and exploitable storages of wave power as presented in Table 6 for both historical and future periods.

Table 6. Historical and future computations of total and exploitable wave power

Climate	Parameter	Jask	Chabahar	Beris	Pasabandar
Hist.	P_{ave} (kW/m)	1.39	11.02	9.01	10.87
	E_t (kWh/m)	12186	96547	78934	95192
	t_e (hr)	396.2	1000.1	971.8	1011.3
	E_e (kWh/m)	551	11022	8757	10989
	Exploitability %	5%	11%	11%	12%
SSP5-8.5	P_{ave} (kW/m)	2.01	13.58	10.89	13.43
	E_t (kWh/m)	17633	118946	95390	117651
	t_e (hr)	448.4	1017.3	1008.2	1045.4
	E_e (kWh/m)	903	13813	10978	14040
	Exploitability %	5%	12%	12%	12%

The results presented in Table 6 show an increasing trend in total and exploitable wave power under SSP5-8.5. An average increase of about 26% in exploitable energy for the three eastern sites is obtained under the future SSP. In addition, a remarkable difference can be detected in total and exploitable wave energy, where the exploitable energy can be about 12% of the total energy in some locations. In the other locations, it can be found as 5%. Considering mean annual values of wave power, it is expected that the wave power values are to be increased according to SSP5-8.5. Regarding the wave power variation for the different locations, it can be inferred that the eastern regions have higher potential than the western areas. For example, the wave power in Pasabandar has a magnitude of about 6.7 and 7.8 times the corresponding values in Jask for the historical and the future periods, respectively. The seasonal distribution of wave energy can provide additional details to the wave energy assessment considering the variability of energy demand and supply.

3.4. Seasonal and monthly variability of historical and future wave power

Temporal variation of wave energy is required to investigate the stability of resources in the short term. Fig. 7 depicts the seasonal variability of wave power for the different locations in the historical and future periods.

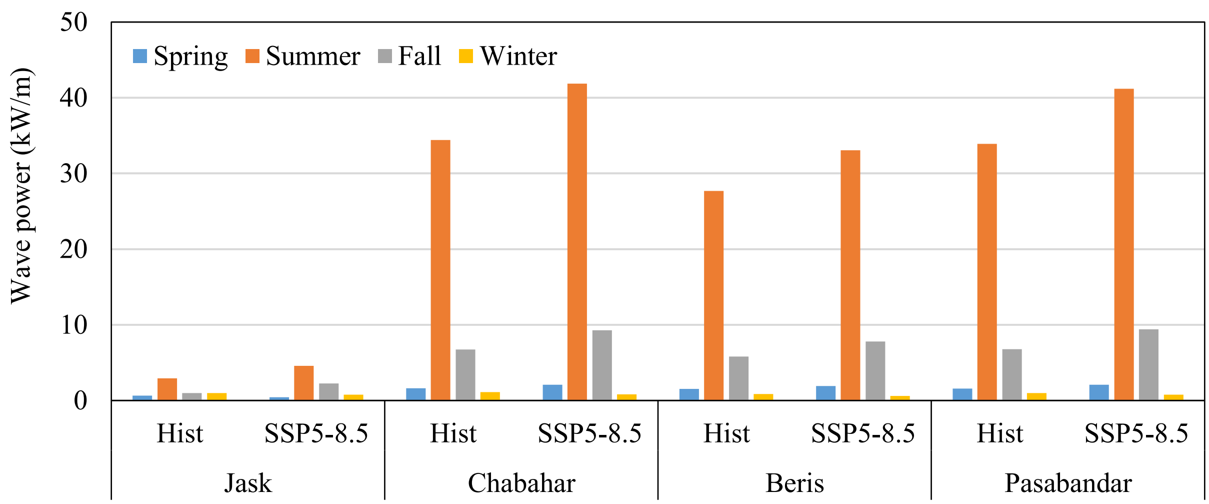

Fig 7. Seasonal variability of wave power for the historical (1981-2000) and future (2081-2100) periods

According to Fig. 7, considerable seasonal variability in wave power can be seen. Generally, in all the stations, the highest energy exists in the summer, while fall ranks the second season in terms of the highest wave power. The pattern of public circulation in this region is significantly influenced by summer and winter monsoons driven by the latent temperature difference between land and sea. The Winter monsoon occurs from November to April and is accompanied by northeast winds with an average speed of below 5 meters per second. Summer monsoon (July-September) causes energetic and continuous winds in the south and southwest with an average speed of 15 meters per second. During the summer, this constant wind regime significantly contributes to ocean circulation and biochemical processes in the northern Arabian Sea and the Gulf of Oman. The remaining months, either after the monsoon (October) or before the monsoon (May and June), are considered with a lesser transition phase and stable wind pattern. Analysis of annual wind data from the Gulf of Oman and the northern Arabian Sea shows that the predominant wind direction in the Gulf of Oman is from west to northwest, while in the Arabian Sea, the southwest direction is dominant [51].

As it can be seen in Fig. 7, the wave energy increases in this scenario. In winter, on the other hand, the wave energy decreases in reverse. This somehow confirms that the Monsoon cycle can be intensified. According to seasonal variability assessment, wave power increases in SPP5-8.5 scenario in spring, summer, and fall by about 13%, 30%, and 59%, respectively. However, it decreases about 24 percent in winter on average in four stations.

During the summertime in the northern hemisphere, summer monsoons blow southwest and generate strong, consistent waves [52]. During the summer monsoons, the western coasts of India experience wave heights up to 6 *m*, whereas in other seasons, the significant wave height is about 1.5 *m* [53]. Similar trends have been demonstrated in the previous studies outlining wind and wave climate in the Gulf of Oman [51,54]. On the contrary, the wave power reaches the lowest values during winter and spring. This finding is promising to have higher wave energy in summer when the demand for the energy supply increases due to hot weather conditions in summers. In this regard, it is worth mentioning that the energy consumption for indoor space cooling (air conditioning) has a large share of energy consumption in the northern land of the study area. Therefore, an excess demand for energy in summer is possible due to the higher temperatures. Hence, wave energy as a supplementary energy supply can be considered.

The future wave power under SSP5-8.5 is higher than the historical values indicating an increase of 21-45% in the future. *P4* and *P2* have relatively higher wave energy than the other stations. Since the seasonal variability is considerable in the study area, assessing intra-annual variation on a monthly scale seems necessary. Hence, the monthly variation of the wave energy is illustrated in Fig. 8.

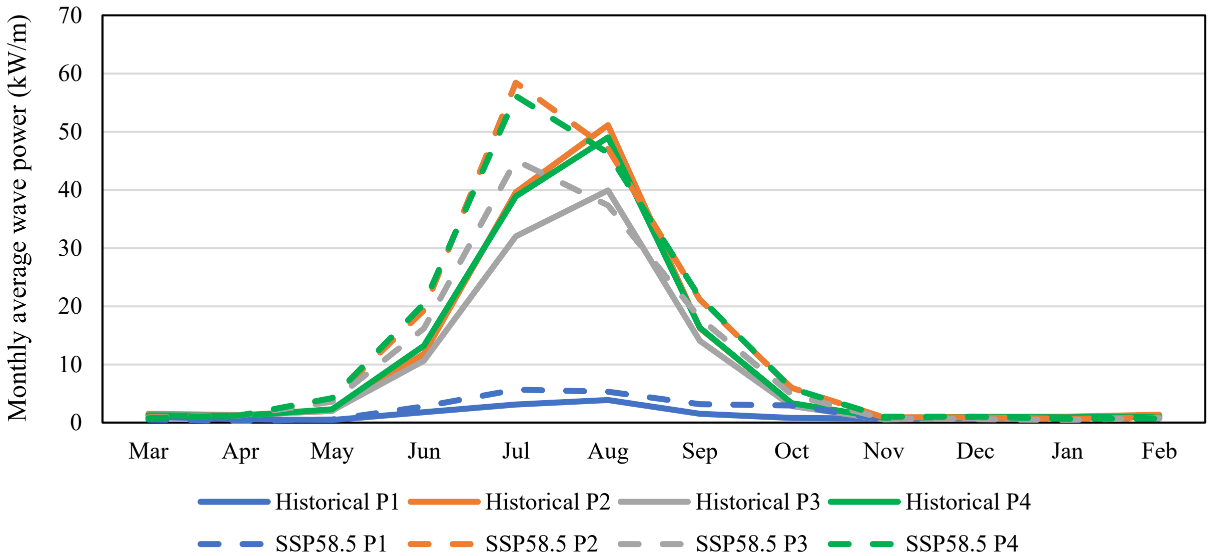

Fig 8. Monthly variation of wave power in the selected stations for the historical (1981-2000) and future (2081-2100) periods

The monthly variability of wave power (Fig. 8) reveals that July and August are among the highest energetic months, while the months in winter and fall have the lowest energy potential. In general, a high variation of wave power in different months can be detected, which is not desirable in terms of the sustainability of energy on the intra-annual scale. Comparison of the results of the historical and future periods shows that the future projections have higher values than historical ones. In order to quantitatively assess the intra-annual variability, historical and future *MVI* and *SVI* values are shown in Fig. 9.

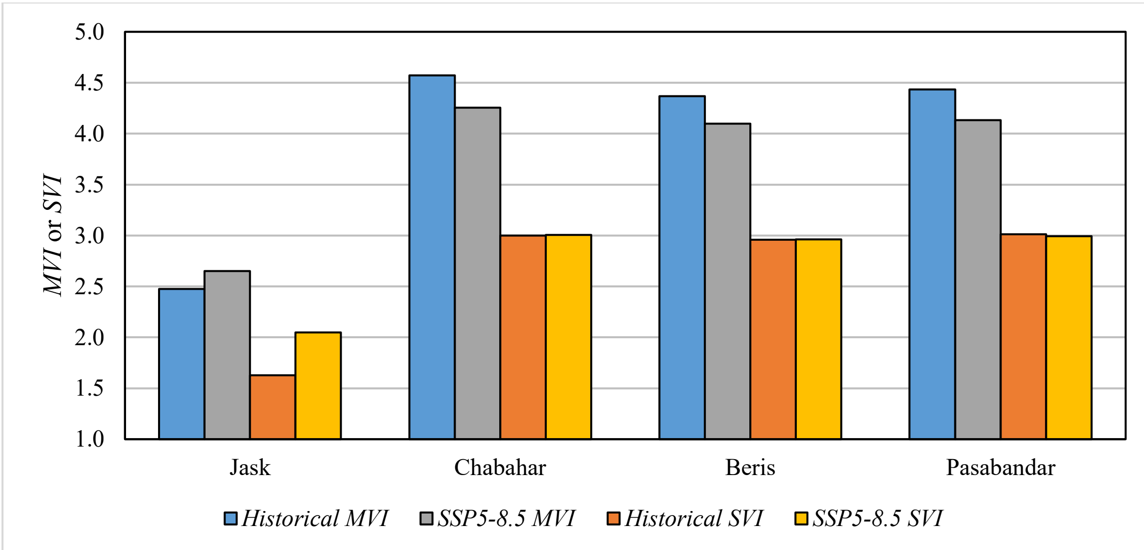

Fig. 9. *MVI* and *SVI* values for the historical (1981-2000) and future (2081-2100) periods

Regarding Fig. 9, Jask has the most stable conditions in terms of monthly and seasonal variability, with the lowest *MVI* and *SVI* values for both historical and future periods. Other stations have higher *MVI* and *SVI*, which is not in favor of wave power stability. However, in Pasabandar, which wave power is remarkable, the variability indices are desirable to guarantee sustainability and availability of the power during different seasons. Since the high values for these indices are initiated by extremely high power in summer, it can be promising due to the increasing demand for electricity in summer when hot weather and more activities are expected. Therefore, the wave power may be considered an opportunity to compensate for the summer energy shortage for the study area. Finally, accessibility and availability of the wave power under the future high emission scenario are needed to be considered for operational purposes. More details have been discussed in the following sub-section.

3.4. Accessibility and availability of wave power under SSP5-8.5

Part of the assessment of wave energy is defined by the accessibility for operation and maintenance of the installations (e.g., Wave Energy Convertors (WECs)). Along with accessibility, the availability of the extractable wave energy is another sea state specification that is required to be taken into account. The criterion specifying the sea state conditions is considered in terms of significant wave height. Moreover, several extreme events may yield high computational wave power, but not in favor of the operation of WECs. This is investigated as the percentage of the hours lying in cut-in and cut-off wave heights to the total hours. In this study, cut-in and cut-off values for significant wave height are 0.5 *m* and 4 *m*, respectively [50]. Table 7 represents the accessibility and availability values in different locations and future periods (SSP5-8.5).

Table 7. Annual and seasonal accessibility and availability of the wave characteristics in each station

Station	Season	Accessibility %							Availability %
		Hs<1.0	*Hs*<1.5	*Hs*<2.0	*Hs*<2.5	*Hs*<3.0	*Hs*<3.5	*Hs*<4.0	0.5<*Hs*<4.0
Jask	Total	79.8	96.0	99.1	99.7	99.9	100.0	100.0	62.8
	Spring	91.1	97.9	99.5	99.8	99.9	100.0	100.0	51.2
	Summer	49.0	92.1	99.3	100.0	100.0	100.0	100.0	99.1
	Fall	91.6	99.4	100.0	100.0	100.0	100.0	100.0	52.0
	Winter	88.0	94.8	97.8	99.1	99.7	100.0	100.0	48.5
Chabahar	Total	51.7	67.5	76.9	84.9	93.2	99.1	100.0	81.0
	Spring	62.3	88.1	98.1	99.4	100.0	100.0	100.0	84.3
	Summer	0.2	5.5	16.2	42.2	73.3	96.5	99.9	99.9
	Fall	57.5	81.9	96.1	99.3	100.0	100.0	100.0	83.5
	Winter	87.7	95.3	97.9	99.2	99.8	100.0	100.0	55.8
Beris	Total	55.1	71.1	79.8	87.8	96.3	99.9	100.0	76.3
	Spring	66.2	93.2	99.2	99.9	100.0	100.0	100.0	84.7
	Summer	0.5	6.7	24.0	52.3	85.4	99.6	100.0	100.0
	Fall	62.8	88.1	97.3	99.7	100.0	100.0	100.0	79.3
	Winter	91.6	97.2	99.1	99.8	100.0	100.0	100.0	40.3
Pasabandar	Total	52.0	67.2	76.4	84.3	92.1	98.7	100.0	81.2
	Spring	61.8	88.3	99.4	100.0	100.0	100.0	100.0	85.0
	Summer	0.1	3.9	12.5	38.9	68.8	94.9	99.9	99.9
	Fall	56.6	80.1	95.4	99.3	100.0	100.0	100.0	85.1
	Winter	90.2	97.3	98.9	99.5	99.8	100.0	100.0	54.2

According to Table 7, it can be found that for Jask, accessibility is higher than in other locations. Generally, all the locations have accessibility higher than 50%, which is suitable to meet the operation and maintenance of the equipment. These values for significant wave heights of less than

1 m reach 80% or higher during winter, while they decrease under 50% in summer. However, for larger waves but lower than 3.5 or 4 *m*, the accessibility for all locations and seasons converges to 100%. In terms of availability, Pasabandar and Chabahar have the highest availability, indicating a better condition for sustainable wave energy extraction. For Jask and Beris, the availability factor is still higher than 60%. The highest and the lowest availability of energy resources are related to the summer and winter seasons, respectively. Seasonal and total computations of accessibility and availability factors for different locations demonstrate the efficiency of the wave energy extraction for the region.

Fig. 9 shows that with the increase in the availability factor, accessibility usually decreases. The highest accessibility and availability values in different stations belong to Jask in the west and Pasabandar in the east, respectively. Therefore, the point in the western part of the region is more suitable in terms of accessibility, while the eastern parts are more suitable for availability. Hence, it can be found that moving from the western part of the region to the eastern parts, availability increases slightly while accessibility decreases. Considering both factors, the energy potential in all stations is considered satisfactory where accessibility and availability are higher than 50%.

4. Discussion

5. Conclusions

As a source of renewable energy, wave power plays an important role in supplying the increasing electricity demand. Different factors are investigated to define the suitability of a station for wave energy exploitation, including the amount of wave power, exploitable storage of wave energy, availability, accessibility, and the intra-annual fluctuation of the mentioned parameters. Moreover, climate change may remarkably influence the wave energy potential since it is influenced by wind patterns and, consequently, the wave climate. This study employed near-surface wind field simulations from a CMIP6 model, i.e., CNRM, for the historical period and a high emission future projection (SSP5-8.5) to drive the wave model and generate the wave characteristics for two 20-yearly periods (1981- 2000 and 2018-2100). Subsequently, wave power for different locations in the northern strip of the Gulf of Oman was calculated. Before performing the numerical wave modeling, a new statistical bias-correction technique based on the Weibull distribution was proposed to modify CNRM wind field compared with ERA-5 dataset. The main findings of this study can be summarized as follow.

- The proposed bias-correction technique partially improved the performance of the existing bias-correction method in additive form. It was found that using the multiplicative form to modify Weibull parameters can be considered as an alternative to the additive form.
- Wave power is drastically higher in summer than in other seasons, indicating a significant temporal and seasonal variability in wave power distribution.
- Under a high emission scenario, an increase in a range of 21-45% in the annual wave power is estimated in the study area. The relative intensification of wave power is greater in the western part (Jask station).
- Under a high emission scenario, wave energy increases in spring, summer, and fall by 13%, 30%, and 59 %, respectively. Conversely, wave power decreases about 24% in winter when averaged over the four stations.
- All the stations have availability and accessibility factors higher than 50%, demonstrating the suitability of the stations for wave energy extraction and wave energy converter installation. According to the results, accessibility increases 4 % in SSP5-8.5.
- Exploitable wave energy increases as total wave energy is between 15 and 23 %, depending on the station.

This study demonstrated a high spatio-temporal variability with an increasing trend in wave power under a future warmer climate. However, summer is the season with the highest energy, which is promising due to the increasing energy demand. Moreover, it was revealed that wave power will increase slightly in the future. The exploitable storage of wave energy exceeds 14MWh in the study area. Results of this study indicating the suitable potential of wave energy and its sustainability can provide useful information for wave energy developers to consider this type of renewable energy for rural and urban regions nearby the gulf. The growing energy demand may lead to joint wind-wave energy (eventually also solar) resource exploitation, increasing the competitiveness of ocean energy.

Acknowledgment

The authors are thankful to the DHI Group for providing us with the student license of MIKE 21 SW. B.K. has been supported by the Hakubi Center for Advanced Research at Kyoto University, and JSPS Grants-in-Aid for Scientific Research (KAKENHI), grant No. 20K04705, supported by the Ministry of Education, Culture, Sports, Science, and Technology of Japan (MEXT).

References

[1] M. Şan, A. Akpınar, B. Bingölbali, M. Kankal, Geo-spatial multi-criteria evaluation of wave energy exploitation in a semi-enclosed sea, Energy. (2021). https://doi.org/10.1016/j.energy.2020.118997.

[2] J. Portilla, J. Sosa, L. Cavaleri, Wave energy resources: Wave climate and exploitation, Renew. Energy. (2013). https://doi.org/10.1016/j.renene.2013.02.032.

[3] A.G. Majidi, B. Bingölbali, A. Akpınar, E. Rusu, Wave power performance of wave energy converters at high-energy areas of a semi-enclosed sea, Energy. 220 (2021) 119705. https://doi.org/https://doi.org/10.1016/j.energy.2020.119705.

[4] A. Ulazia, G. Esnaola, P. Serras, M. Penalba, On the impact of long-term wave trends on the geometry optimisation of oscillating water column wave energy converters, Energy. (2020). https://doi.org/10.1016/j.energy.2020.118146.

[5] M.J. Alizadeh, T. Alinejad-Tabrizi, M.R. Kavianpour, S. Shamshirband, Projection of spatiotemporal variability of wave power in the Persian Gulf by the end of 21st century: GCM and CORDEX ensemble, J. Clean. Prod. (2020). https://doi.org/10.1016/j.jclepro.2020.120400.

[6] J.P. Sierra, M. Casas-Prat, E. Campins, Impact of climate change on wave energy resource: The case of Menorca (Spain), Renew. Energy. (2017). https://doi.org/10.1016/j.renene.2016.08.060.

[7] L. Rusu, Evaluation of the near future wave energy resources in the Black Sea under two

climate scenarios, Renew. Energy. (2019). https://doi.org/10.1016/j.renene.2019.04.092.

[8] M.V.W. Cuttler, J.E. Hansen, R.J. Lowe, Seasonal and interannual variability of the wave climate at a wave energy hotspot off the southwestern coast of Australia, Renew. Energy. (2020). https://doi.org/10.1016/j.renene.2019.08.058.

[9] D. Iribarren, M. Martín-Gamboa, Z. Navas-Anguita, D. García-Gusano, J. Dufour, Influence of climate change externalities on the sustainability-oriented prioritisation of prospective energy scenarios, Energy. (2020). https://doi.org/10.1016/j.energy.2020.117179.

[10] B.G. Reguero, I.J. Losada, F.J. Méndez, A recent increase in global wave power as a consequence of oceanic warming, Nat. Commun. (2019). https://doi.org/10.1038/s41467-018-08066-0.

[11] A. Ulazia, M. Penalba, G. Ibarra-Berastegui, J. Ringwood, J. Saénz, Wave energy trends over the Bay of Biscay and the consequences for wave energy converters, Energy. (2017). https://doi.org/10.1016/j.energy.2017.09.099.

[12] A. Martinez, G. Iglesias, Wind resource evolution in Europe under different scenarios of climate change characterised by the novel Shared Socioeconomic Pathways, Energy Convers. Manag. 234 (2021) 113961. https://doi.org/https://doi.org/10.1016/j.enconman.2021.113961.

[13] A. Martinez, G. Iglesias, Climate change impacts on wind energy resources in North America based on the CMIP6 projections, Sci. Total Environ. 806 (2022) 150580. https://doi.org/https://doi.org/10.1016/j.scitotenv.2021.150580.

[14] R. Le Roux, M. Katurji, P. Zawar-Reza, H. Quénol, A. Sturman, Comparison of statistical and dynamical downscaling results from the WRF model, Environ. Model. Softw. (2018). https://doi.org/10.1016/j.envsoft.2017.11.002.

[15] M.J. Alizadeh, M.R. Kavianpour, B. Kamranzad, A. Etemad-Shahidi, A Weibull Distribution Based Technique for Downscaling of Climatic Wind Field, Asia-Pacific J. Atmos. Sci. (2019). https://doi.org/10.1007/s13143-019-00106-z.

[16] B. Liu, K.B. Costa, L. Xie, F.H.M. Semazzi, Dynamical downscaling of climate change impacts on wind energy resources in the contiguous United States by using a limited-area model with scale-selective data assimilation, Adv. Meteorol. (2014). https://doi.org/10.1155/2014/897246.

[17] J. Ringwood, G. Brandle, A new world map for wave power with a focus on variability, in: Proc. 11th Eur. Wave Tidal Energy Conf., European Wave and Tidal Energy Conference 2015, 2015.

[18] R.G. Coe, S. Ahn, V.S. Neary, P.H. Kobos, G. Bacelli, Maybe less is more: Considering capacity factor, saturation, variability, and filtering effects of wave energy devices, Appl. Energy. (2021). https://doi.org/10.1016/j.apenergy.2021.116763.

[19] D. Khojasteh, D. Khojasteh, R. Kamali, A. Beyene, G. Iglesias, Assessment of renewable energy resources in Iran; with a focus on wave and tidal energy, Renew. Sustain. Energy Rev. 81 (2018) 2992–3005. https://doi.org/https://doi.org/10.1016/j.rser.2017.06.110.

[20] A. Saket, A. Etemad-Shahidi, Wave energy potential along the northern coasts of the Gulf of Oman, Iran, Renew. Energy. (2012). https://doi.org/10.1016/j.renene.2011.09.024.

[21] B. Kamranzad, V. Chegini, A. Etemad-Shahidi, Temporal-spatial variation of wave energy and nearshore hotspots in the Gulf of Oman based on locally generated wind waves, Renew. Energy. (2016). https://doi.org/10.1016/j.renene.2016.03.084.

[22] B. Kamranzad, S. Hadadpour, A multi-criteria approach for selection of wave energy converter/location, Energy. 204 (2020) 117924. https://doi.org/https://doi.org/10.1016/j.energy.2020.117924.

[23] DHI, MIKE 21 SW - Spectral Wave Model: Scientific Documentation, DHI Water Environ. (2014).

[24] A.S. Ribeiro, M. deCastro, X. Costoya, L. Rusu, J.M. Dias, M. Gomez-Gesteira, A Delphi method to classify wave energy resource for the 21st century: Application to the NW Iberian Peninsula, Energy. (2021). https://doi.org/10.1016/j.energy.2021.121396.

[25] H. Hersbach, B. Bell, P. Berrisford, S. Hirahara, A. Horányi, J. Muñoz-Sabater, J. Nicolas,

C. Peubey, R. Radu, D. Schepers, A. Simmons, C. Soci, S. Abdalla, X. Abellan, G. Balsamo, P. Bechtold, G. Biavati, J. Bidlot, M. Bonavita, G. De Chiara, P. Dahlgren, D. Dee, M. Diamantakis, R. Dragani, J. Flemming, R. Forbes, M. Fuentes, A. Geer, L. Haimberger, S. Healy, R.J. Hogan, E. Hólm, M. Janisková, S. Keeley, P. Laloyaux, P. Lopez, C. Lupu, G. Radnoti, P. de Rosnay, I. Rozum, F. Vamborg, S. Villaume, J.N. Thépaut, The ERA5 global reanalysis, Q. J. R. Meteorol. Soc. (2020). https://doi.org/10.1002/qj.3803.

[26] R. Seferian, CNRM-CERFACS CNRM-ESM2-1 model output prepared for CMIP6 CMIP, (2018). https://doi.org/10.22033/ESGF/CMIP6.1391.

[27] K. Mahmoodi, H. Ghassemi, A. Razminia, Temporal and spatial characteristics of wave energy in the Persian Gulf based on the ERA5 reanalysis dataset, Energy. (2019). https://doi.org/10.1016/j.energy.2019.115991.

[28] M. Beyramzadeh, S.M. Siadatmousavi, M.H. Derkani, Calibration and skill assessment of two input and dissipation parameterizations in WAVEWATCH-III model forced with ERA5 winds with application to Persian Gulf and Gulf of Oman, Ocean Eng. (2021). https://doi.org/10.1016/j.oceaneng.2020.108445.

[29] M.J. Alizadeh, M.R. Kavianpour, B. Kamranzad, A. Etemad-Shahidi, A distributed wind downscaling technique for wave climate modeling under future scenarios, Ocean Model. 145 (2020) 101513. https://doi.org/10.1016/j.ocemod.2019.101513.

[30] A. Patra, P.K. Bhaskaran, Temporal variability in wind–wave climate and its validation with ESSO-NIOT wave atlas for the head Bay of Bengal, Clim. Dyn. (2017). https://doi.org/10.1007/s00382-016-3385-z.

[31] M. Wandres, C. Pattiaratchi, Y. Hetzel, E.M.S. Wijeratne, The response of the southwest Western Australian wave climate to Indian Ocean climate variability, Clim. Dyn. (2018). https://doi.org/10.1007/s00382-017-3704-z.

[32] B.C. O'Neill, C. Tebaldi, D.P. Van Vuuren, V. Eyring, P. Friedlingstein, G. Hurtt, R. Knutti, E. Kriegler, J.F. Lamarque, J. Lowe, G.A. Meehl, R. Moss, K. Riahi, B.M. Sanderson, The Scenario Model Intercomparison Project (ScenarioMIP) for CMIP6,

Geosci. Model Dev. (2016). https://doi.org/10.5194/gmd-9-3461-2016.

[33] A. Lira-Loarca, F. Ferrari, A. Mazzino, G. Besio, Future wind and wave energy resources and exploitability in the Mediterranean Sea by 2100, Appl. Energy. (2021). https://doi.org/10.1016/j.apenergy.2021.117492.

[34] A. Ahmadalipour, A. Rana, H. Moradkhani, A. Sharma, Multi-criteria evaluation of CMIP5 GCMs for climate change impact analysis, Theor. Appl. Climatol. (2017). https://doi.org/10.1007/s00704-015-1695-4.

[35] A. Voldoire, D. Saint-Martin, S. Sénési, B. Decharme, A. Alias, M. Chevallier, J. Colin, J. -F. Guérémy, M. Michou, M. -P. Moine, P. Nabat, R. Roehrig, D. y Mélia, R. Séférian, S. Valcke, I. Beau, S. Belamari, S. Berthet, C. Cassou, J. Cattiaux, J. Deshayes, H. Douville, C. Ethé, L. Franchistéguy, O. Geoffroy, C. Lévy, G. Madec, Y. Meurdesoif, R. Msadek, A. Ribes, E. Sanchez-Gomez, L. Terray, R. Waldman, Evaluation of {CMIP6} {DECK} {Experiments} {With} {CNRM}-{CM6}-1, J. Adv. Model. Earth Syst. 11 (2019) 2177–2213. https://doi.org/10.1029/2019MS001683.

[36] A. Ouammi, R. Sacile, D. Zejli, A. Mimet, R. Benchrifa, Sustainability of a wind power plant: Application to different Moroccan sites, Energy. (2010). https://doi.org/10.1016/j.energy.2010.07.010.

[37] I.A. Anton, L. Rusu, C. Anton, Nearshore wave dynamics at Mangalia beach simulated by spectral models, J. Mar. Sci. Eng. (2019). https://doi.org/10.3390/jmse7070206.

[38] M.A. Hoque, W. Perrie, S.M. Solomon, Evaluation of two spectral wave models for wave hindcasting in the Mackenzie Delta, Appl. Ocean Res. (2017). https://doi.org/10.1016/j.apor.2016.11.009.

[39] M.H. Moeini, A. Etemad-Shahidi, Application of two numerical models for wave hindcasting in Lake Erie, Appl. Ocean Res. (2007). https://doi.org/10.1016/j.apor.2007.10.001.

[40] P.G. Remya, R. Kumar, S. Basu, A. Sarkar, Wave hindcast experiments in the Indian Ocean using MIKE 21 SW model, J. Earth Syst. Sci. (2012).

https://doi.org/10.1007/s12040-012-0169-7.

[41] R.C. Ris, L.H. Holthuijsen, N. Booij, A third-generation wave model for coastal regions 2. Verification, J. Geophys. Res. Ocean. (1999). https://doi.org/10.1029/1998jc900123.

[42] G.J. Komen, L. Cavaleri, M. Donelan, K. Hasselmann, S. Hasselmann, P.A.E.M. Janssen, Dynamics and Modelling of Ocean Waves, 1994. https://doi.org/10.1017/cbo9780511628955.

[43] M.J. Tucker, E.G. Pitt, Waves in ocean engineering, (2001). http://books.google.com/books?id=0v5RAAAAMAAJ.

[44] R.E. and A.U.P. (U.S.), Technology white paper on wave energy potential on the U.S. Outer Continental Shelf., (2006). https://purl.fdlp.gov/GPO/LPS94821.

[45] B. Kamranzad, S. Hadadpour, A multi-criteria approach for selection of wave energy converter/location, Energy. 204 (2020) 117924. https://doi.org/https://doi.org/10.1016/j.energy.2020.117924.

[46] L. Margheritini, D. Vicinanza, P. Frigaard, SSG wave energy converter: Design, reliability and hydraulic performance of an innovative overtopping device, Renew. Energy. 34 (2009) 1371–1380.

[47] C.W. Zheng, C.Y. Li, X. Chen, J. Pan, Numerical Forecasting Experiment of the Wave Energy Resource in the China Sea, Adv. Meteorol. (2016). https://doi.org/10.1155/2016/5692431.

[48] C.W. Zheng, J. Pan, J.X. Li, Assessing the China Sea wind energy and wave energy resources from 1988 to 2009, Ocean Eng. (2013). https://doi.org/10.1016/j.oceaneng.2013.03.006.

[49] M. Penalba, A. Ulazia, G. Ibarra-Berastegui, J. Ringwood, J. Sáenz, Wave energy resource variation off the west coast of Ireland and its impact on realistic wave energy converters' power absorption, Appl. Energy. (2018). https://doi.org/10.1016/j.apenergy.2018.04.121.

[50] G. Lavidas, A. Agarwal, V. Venugopal, Availability and Accessibility for Offshore

Operations in the Mediterranean Sea, J. Waterw. Port, Coastal, Ocean Eng. (2018). https://doi.org/10.1061/(asce)ww.1943-5460.0000467.

[51] N. Chaichitehrani, M.N. Allahdadi, Overview of Wind Climatology for the Gulf of Oman and the Northern Arabian Sea, Am. J. Fluid Dyn. (2018).

[52] M. Seemanth, S.A. Bhowmick, R. Kumar, R. Sharma, Sensitivity analysis of dissipation parameterizations in a third-generation spectral wave model, WAVEWATCH III for Indian Ocean, Ocean Eng. (2016). https://doi.org/10.1016/j.oceaneng.2016.07.023.

[53] P. Vethamony, K. Sudheesh, S.P. Rupali, M.T. Babu, S. Jayakumar, A.K. Saran, S.K. Basu, R. Kumar, A. Sarkar, Wave modelling for the north Indian Ocean using MSMR analysed winds, Int. J. Remote Sens. 27 (2006) 3767–3780. https://doi.org/10.1080/01431160600675820.

[54] V. Sanil Kumar, J. Singh, P. Pednekar, R. Gowthaman, Waves in the nearshore waters of northern Arabian Sea during the summer monsoon, Ocean Eng. (2011). https://doi.org/10.1016/j.oceaneng.2010.11.009.